Comparing proton momentum distributions in $A = 3$ nuclei via ^{3}He and ^{3}H$(e, e'p)$ measurements

R. Cruz-Torres,[1] S. Li,[2] F. Hauenstein,[3] A. Schmidt,[1] D. Abrams,[4] H. Albataineh,[5] S. Alsalmi,[6] D. Androic,[7] K. Aniol,[8] W. Armstrong,[9] J. Arrington,[9] H. Atac,[10] T. Averett,[11] C. Ayerbe Gayoso,[11] X. Bai,[4] J. Bane,[12] S. Barcus,[11] A. Beck,[1] V. Bellini,[13] H. Bhatt,[14] D. Bhetuwal,[14] D. Biswas,[15] D. Blyth,[9] W. Boeglin,[16] D. Bulumulla,[3] A. Camsonne,[17] J. Castellanos,[16] J-P. Chen,[17] E. O. Cohen,[18] S. Covrig,[17] K. Craycraft,[12] B. Dongwi,[15] M. Duer,[18] B. Duran,[10] D. Dutta,[14] E. Fuchey,[19] C. Gal,[4] T. N. Gautam,[15] S. Gilad,[1] K. Gnanvo,[4] T. Gogami,[20] J. Gomez,[17] C. Gu,[4] A. Habarakada,[21] T. Hague,[6] O. Hansen,[17] M. Hattawy,[9] O. Hen,[1] D. W. Higinbotham,[17] E. Hughes,[22] C. Hyde,[3] H. Ibrahim,[23] S. Jian,[4] S. Joosten,[10] A. Karki,[14] B. Karki,[24] A. T. Katramatou,[6] C. Keppel,[17] M. Khachatryan,[3] V. Khachatryan,[25] A. Khanal,[16] D. King,[26] P. King,[24] I. Korover,[27] K. Kumar,[25] T. Kutz,[25] N. Lashley-Colthirst,[15] G. Laskaris,[1] W. Li,[28] H. Liu,[29] N. Liyanage,[4] D. Lonardoni,[30,31] R. Machleidt,[32] L.E. Marcucci,[33,34] P. Markowitz,[16] E. McClellan,[17] D. Meekins,[17] S. Mey-Tal Beck,[1] Z-E. Meziani,[10] R. Michaels,[17] M. Mihovilovič,[35,36] V. Nelyubin,[4] D. Nguyen,[4] N. Nuruzzaman,[15] M. Nycz,[6] R. Obrecht,[19] M. Olson,[37] L. Ou,[1] V. Owen,[11] B. Pandey,[15] V. Pandey,[38] A. Papadopoulou,[1] S. Park,[25] M. Patsyuk,[1] S. Paul,[11] G. G. Petratos,[6] E. Piasetzky,[18] R. Pomatsalyuk,[39] S. Premathilake,[4] A. Puckett,[19] V. Punjabi,[40] R. Ransome,[41] M. N. H. Rashad,[3] P. E. Reimer,[9] S. Riordan,[9] J. Roche,[24] F. Sammarruca,[32] N. Santiesteban,[2] B. Sawatzky,[17] E. P. Segarra,[1] B. Schmookler,[1] A. Shahinyan,[42] S. Širca,[35,36] N. Sparveris,[43] T. Su,[6] R. Suleiman,[17] H. Szumila-Vance,[17] A. S. Tadepalli,[41] L. Tang,[17] W. Tireman,[44] F. Tortorici,[13] G. Urciuoli,[45] M. Viviani,[34] L. B. Weinstein,[3] B. Wojtsekhowski,[17] S. Wood,[17] Z. H. Ye,[9] Z. Y. Ye,[46] and J. Zhang[25]

(Jefferson Lab Hall A Tritium Collaboration)

[1] *Massachusetts Institute of Technology, Cambridge, MA*
[2] *University of New Hampshire, Durham, NH*
[3] *Old Dominion University, Norfolk, VA*
[4] *University of Virginia, Charlottesville, VA*
[5] *Texas A & M University, Kingsville, TX*
[6] *Kent State University, Kent, OH*
[7] *University of Zagreb, Zagreb, Croatia*
[8] *California State University , Los Angeles, CA*
[9] *Physics Division, Argonne National Laboratory, Argonne, IL*
[10] *Temple University, Philadelphia, PA*
[11] *The College of William and Mary, Williamsburg, VA*
[12] *University of Tennessee, Knoxville, TN*
[13] *INFN Sezione di Catania, Italy*
[14] *Mississippi State University, Miss. State, MS*
[15] *Hampton University , Hampton, VA*
[16] *Florida International University, Miami, FL*
[17] *Jefferson Lab, Newport News, VA*
[18] *School of Physics and Astronomy, Tel Aviv University, Tel Aviv 69978, Israel*
[19] *University of Connecticut, Storrs, CT*
[20] *Tohoku University, Sendai, Japan*
[21] *Liyanage Hampton University , Hampton, VA*
[22] *Columbia University, New York, NY*
[23] *Cairo University, Cairo, Egypt*
[24] *Ohio University, Athens, OH*
[25] *Stony Brook, State University of New York, NY*
[26] *Syracuse University, Syracuse, NY*
[27] *Nuclear Research Center -Negev, Beer-Sheva, Israel*
[28] *University of Regina, Regina, SK , Canada*
[29] *Columbia University ,New York, NY*
[30] *Facility for Rare Isotope Beams, Michigan State University, East Lansing, Michigan 48824, USA*
[31] *Theoretical Division, Los Alamos National Laboratory, Los Alamos, New Mexico 87545, USA*
[32] *Department of Physics, University of Idaho, Moscow, ID 83844, USA*
[33] *Department of Physics "E. Fermi", University of Pisa, Italy*
[34] *INFN, Pisa, Italy*
[35] *University of Ljubljana, Ljubljana, Slovenia*
[36] *Jožef Stefan Institute, Ljubljana, Slovenia*
[37] *Saint Norbert College, De Pere, WI*

[38] Virginia Tech, Blacksburg, VA
[39] Institute of Physics and Technology, Kharkov, Ukraine
[40] Norfolk State University, Norfolk, VA
[41] Rutgers University, New Brunswick, NJ
[42] Artem Alikhanian National Laboratory, Yerevan, Armenia
[43] Tel Aviv University, Tel Aviv, Israel
[44] Northern Michigan University, Marquette, MI
[45] INFN, Rome, Italy
[46] University of Illinois-Chicago, IL

(Dated: February 8, 2019)

We report the first measurement of the $(e, e'p)$ reaction cross-section ratio for Helium-3 (^{3}He) relative to Tritium (^{3}H). The measurement covered a missing momentum range of $40 \leq p_{miss} \leq 550\,\mathrm{MeV}/c$, at large momentum transfer ($\langle Q^2 \rangle \approx 1.9$ (GeV/c)^2) and $x_B > 1$, which minimized contributions from non quasi-elastic (QE) reaction mechanisms. The data is compared with calculations performed within the plane-wave impulse approximation (PWIA) using realistic spectral functions and momentum distributions. The measured and PWIA cross-section ratios agree within the measurement accuracy of about 3% up to the nuclear Fermi-momentum (≈ 250 MeV/c) and differ by 20% − 50% at higher momenta. Final state interaction (FSI) calculations using the generalized Eikonal Approximation indicate that FSI should change the ^{3}He/^{3}H cross-section ratio for this measurement by less than 5%. This suggests that the differences at large missing momenta between the ^{3}He/^{3}H experimental and calculated ratios could be due to the underlying NN interaction, and thus could provide new constraints on the previously loosely-constrained short-distance parts of the NN interaction.

Nuclear interaction models are a crucial starting point for modern calculations of nuclear structure and reactions, as well as the properties of dense astrophysical objects such as neutron stars. Phenomenological or meson-theoretic two-body potentials, such as CD-Bonn and Argonne-V18 (AV18), were developed in the 1990s using constraints primarily from nucleon-nucleon (NN) scattering data [1, 2]. More recently, chiral effective field theory (EFT) has led to the development of potentials with systematic and controlled approximations [3–5]. Light atomic nuclei have played a crucial role in constraining modern nuclear interaction models, including many-body forces, as many of their properties (e.g., charge distributions and radii, ground- and excited-state energies) can be both precisely measured and exactly calculated for a given two- and three-nucleon interaction model [6–10].

While the combination of NN scattering and light-nuclei data allows one to constrain the two- and three-nucleon interaction at large distances, its short-ranged behavior is still largely unconstrained. The latter is important for understanding nucleon-nucleon short-range correlations (SRC) in nuclei [11, 12], their relation to the partonic structure of bound nucleons [13–17], and the structure of neutron stars [18, 19].

Constraining the short-ranged part of the nuclear interaction requires studying nuclear momentum distributions at high-momentum. However, previous attempts to extract these were largely unsuccessful, due to the fact that nuclear momentum distributions are not direct observables, and typical experimental extractions suffer from large reaction mechanism effects. These introduce significant model-dependent corrections that mask the underlying characteristics of the momentum distribution, especially at high-momentum [20–23].

Advances in nuclear reaction theory now allow us to identify observables with increased sensitivity to nuclear momentum densities at high-momentum [18, 24–27]. In light of these advances, we report on a new study of the momentum distribution of nucleons in Helium-3 relative to Tritium over a broad momentum range.

We study nucleon momentum distributions using Quasi-Elastic (QE) electron scattering. In these experiments, an electron with momentum $\vec{p}_e$ is scattered from the nucleus, transferring energy ω and momentum $\vec{q}$ to the nucleus. We choose ω and $\vec{q}$ to be appropriate for elastic scattering from a moving bound nucleon. By detecting the knocked-out proton ($\vec{p}_p$) in coincidence with the scattered electron ($\vec{p}_e{}'$), we can measure the missing energy and missing momentum of the reaction:

$$E_{miss} = \omega - T_p - T_{A-1}, \tag{1}$$

$$\vec{p}_{miss} = \vec{p}_p - \vec{q}, \tag{2}$$

where $\vec{q} = \vec{p}_e - \vec{p}_e{}'$ is the momentum transfer, $T_{A-1} = (\omega + m_A - E_p) - \sqrt{(\omega + m_A - E_p)^2 - |\vec{p}_{miss}|^2}$ is the reconstructed kinetic energy of the residual $A-1$ system, and T_p and E_p are the measured kinetic and total energies of the outgoing proton.

In the Plane-Wave Impulse Approximation (PWIA) for QE scattering, where a single exchanged photon is absorbed on a single proton and the knocked-out proton does not re-interact as it leaves the nucleus, the cross-section for $A(e, e'p)$, electron-induced proton knockout from nucleus A, can be written as [28, 29]:

$$\frac{d^6\sigma}{d\omega dE_p d\Omega_e d\Omega_p} = K\sigma_{ep} S(|\vec{p}_i|, E_i) \tag{3}$$

where σ_{ep} is the cross-section for scattering an electron from a bound proton [29], $K = E_p|\vec{p}_p|$ is a kinematical factor, $d\Omega_e$ and $d\Omega_p$ are the electron and proton solid angles respectively, and $S(|\vec{p}_i|, E_i)$ is the spectral function, which defines the probability to find a proton in the nucleus with momentum $|\vec{p}_i|$ and separation energy E_i. The nuclear momentum distribution is the integral of the spectral function over the separation energy: $n(|\vec{p}_i|) = \int S(|\vec{p}_i|, E_i)dE_i$.

In PWIA, the missing momentum and energy equal the initial momentum and separation energy of the knocked-out nucleon: $\vec{p}_i = \vec{p}_{miss}$, $E_i = E_{miss}$. However, there are other, non-QE, reaction mechanisms, including final state interactions (the rescattering of the knocked-out proton, FSI), scattering from a meson-exchange current (MEC), and exciting isobar configurations (IC) that can lead to the same measured final state. These also contribute to the cross section, complicating this simple picture.

Previous measurements of the ^{3}He$(e, e'p)$ two- and three-body breakup cross-sections were done at $Q^2 = 1.5$ (GeV/c)^2 and $x_B \equiv \frac{Q^2}{2m_p\omega} = 1$ where m_p is the proton mass [21, 22], near the expected maximum of the proton rescattering. The measured cross-sections disagreed by up to a factor of five with PWIA calculations for $p_{miss} > 250$ MeV/c. These deviations were described to good accuracy by calculations which included the contribution of non-QE reaction mechanisms, primarily FSI [18, 24–26]. The large contribution of such non-QE reaction mechanisms to the measured $(e, e'p)$ cross-sections limited their ability to constrain the nuclear momentum distribution at high momenta.

Guided by reaction mechanism calculations, which agree with previous measurements, we can reduce the effect of FSI in two ways [25, 27, 30–34] by: (A) constraining the angle between $\vec{p}_{recoil} = -\vec{p}_{miss}$ and $\vec{q}$ to be $\theta_{rq} \lesssim 40°$ and (B) taking the ratio of $(e, e'p)$ cross-sections for same-mass nuclei. The effect of FSI should be similar in both nuclei because knocked-out protons in both nuclei can rescatter from the same number of nucleons and FSI should therefore largely cancel in the ratio.

Additional non-QE reaction mechanisms such MEC and IC were shown to be suppressed for $Q^2 \equiv q^2 - \omega^2 >$ 1.5 (GeV/c)^2 and $x_B > 1$ [30, 35]. Thus, the ratio of ^{3}He$(e, e'p)$ to ^{3}H$(e, e'p)$ cross-sections in QE kinematics at $Q^2 > 1.5$ (GeV/c)^2, $x_B > 1$ and $\theta_{rq} \lesssim 40°$ should have increased sensitivity to the ratio of their spectral functions.

We measured the ratio of ^{3}He$(e, e'p)$ to ^{3}H$(e, e'p)$ cross-sections in Hall A of the Thomas Jefferson National Accelerator Facility (JLab) using the two high-resolution spectrometers (HRS) and a 20 μA 4.326 GeV electron beam incident on one of four 25-cm long gas target cells [36]. The four identical cells were filled with Hydrogen (70.8 ± 0.4 mg/cm^2), Deuterium

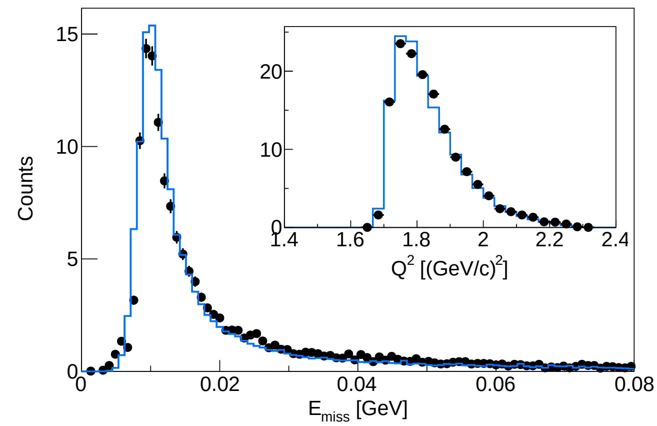

FIG. 1. (color online) Number of ^{3}H$(e, e'p)$ events (counts) versus missing energy for the low p_{miss} kinematics. The black markers correspond to the measured data. The lines correspond to the calculated distributions obtained from a SIMC [38] simulation with a spectral function calculated by C. Ciofi degli Atti and L. P. Kaptari [39] normalized to the data. The insert shows the Q^2 distribution for the same kinematical setting.

(142.2 ± 0.8 mg/cm^2), ^{3}He (53.4 ± 0.6 mg/cm^2) and Tritium (85.1 ± 0.8 mg/cm^2) gas [37]. We detected the scattered electrons in the left HRS at a central angle $\theta_e = 20.88°$ and momentum $p_e = 3.543$ GeV/c, corresponding to a central four-momentum transfer $Q^2 = 2.0$ (GeV/c)^2, energy transfer $\omega = 0.78$ GeV, and $x_B = 1.4$. We detected the knocked-out protons in the right HRS at two different kinematical settings, $(\theta_p, p_p) = (48.82°$, 1.481 GeV/c), and (58.50°, 1.246 GeV/c), referred to here as "low p_{miss}" and "high p_{miss}" respectively. These two settings cover a combined missing momentum range of $40 \le p_{miss} \le 550$ MeV/c.

Each HRS consists of three quadrupole magnets for focusing and one dipole magnet for momentum analysis [40, 41]. These magnets are followed by a detector package, slightly updated with respect to the one in Ref [40], consisting of a pair of vertical drift chambers used for tracking, and two scintillation counter planes that provide timing and trigger signals. A CO_2 Cherenkov detector placed between the scintillators and a lead-glass calorimeter placed after them are used for particle identification.

Electrons were selected by requiring that the particle deposits more than half of its energy in the calorimeter: $\frac{E_{cal}}{|\vec{p}|} > 0.5$. $(e, e'p)$ coincidence events were selected by placing a $\pm 3\sigma$ cut around the relative electron and proton event times. Due to the low experimental luminosity, the random coincidence event rate was negligible. We discarded a small number of runs with anomalous numbers of events normalized to the beam charge.

Measured electrons were required to originate within the central ± 9 cm of the gas target to exclude scattering events originating from the target walls. The electron and proton reconstructed target vertices were required to be within ±1.2 cm of each other, which corresponds to $\pm3\sigma$ of the vertex reconstruction resolution. By measuring scattering from an empty-cell-like target we determined that the target cell wall contribution to the measured $(e, e'p)$ event yield is negligible ($\ll 1\%$).

To avoid the acceptance edges of the spectrometer, we restricted the analysis to events that are detected within ±4% of the central spectrometer momentum, and ±27.5 mrad in in-plane angle and ±55.0 mrad in out-of-plane angle relative to the center of the spectrometer acceptance. In addition, we further restricted the measurement phase-space by requiring $\theta_{rq} < 37.5°$ to minimize the effect of FSI and, in the high p_{miss} kinematics, $x_B > 1.3$ to further suppress non-QE events.

The spectrometers were calibrated using sieve slit measurements to define scattering angles and by measuring the kinematically over-constrained exclusive $\mathrm{H}(e, e'p)$ and $^2\mathrm{H}(e, e'p)n$ reactions. The $\mathrm{H}(e, e'p)$ reaction p_{miss} resolution was found to be better than 9 MeV/c. We verified the absolute luminosity normalization by comparing the measured elastic $\mathrm{H}(e, e')$ yield to a parametrization of the world data [42]. We also found excellent agreement between the elastic $\mathrm{H}(e, e'p)$ and $\mathrm{H}(e, e')$ rates, confirming that the coincidence trigger performed efficiently.

Figure 1 shows the number of measured $^3\mathrm{H}(e, e'p)$ events as a function of E_{miss} and of Q^2 for the low p_{miss} setting as well as the same distributions calculated using the Monte Carlo code SIMC [38] and normalized to the data. The latter generated $(e, e'p)$ events using Eq. 3, with the addition of radiation effects, that were then propagated through the spectrometer model to account for acceptance and resolution effects, and subsequently analyzed as the data. The SIMC calculations used a ^{3}He spectral function calculated by C. Ciofi degli Atti and L. P. Kaptari using the AV18 potential [39]. Due to the lack of ^{3}H proton spectral functions, we assumed isospin symmetry and used the ^{3}He neutron spectral function for the $^3\mathrm{H}(e, e'p)$ simulation. The difference between the calculated momentum distributions of neutrons in ^{3}He and protons in ^{3}H is small and contributes a 3% uncertainty to the $^3\mathrm{H}(e, e'p)$ calculations and to the spectral-function ratio calculations [43]. The spectral function calculation appears to describe the measured Q^2 and E_{miss} distributions well. See online supplementary materials for details and additional comparisons.

For each nucleus, we calculated the normalized $(e, e'p)$ event yield as:

$$Y_{\mathrm{A}}(p_{miss}) = \frac{N(p_{miss})}{C \cdot t_{\mathrm{live}} \cdot \rho \cdot b},$$

where A stands for ^{3}He or ^{3}H, $N(p_{miss})$ is the number of counts for that target in a given bin of p_{miss} integrated over the experimental E_{miss} acceptance, C is the total accumulated beam charge, t_{live} is the live time fraction in which the detectors are able to collect data, ρ is the nominal areal density of the gas in the target cell, and b is a correction factor to account for changes in the target density caused by local beam heating. The latter was detemined by measuring the beam current dependence of the inclusive event yield [37].

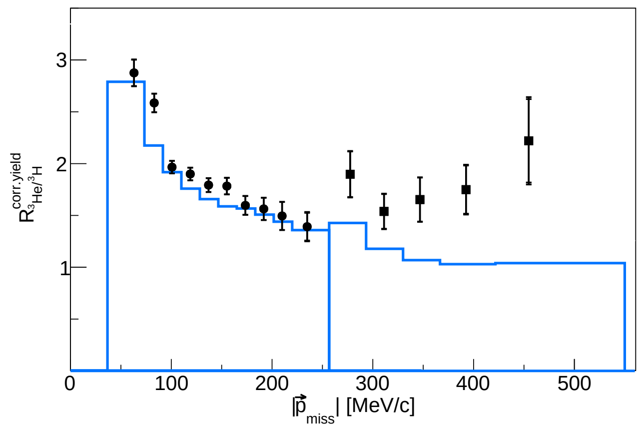

FIG. 2. Missing momentum dependence of the measured ^{3}He/$^3\mathrm{H}(e, e'p)$ normalized event yields ratio $R^{corr.yield}_{^3\mathrm{He}/^3\mathrm{H}}$. The circles and squares correspond to the low and high p_{miss} settings respectively. The error bars include both statistical and point-to-point systematical uncertainties. An additional overall normalization uncertainty of 1.8% is not shown (see Table I). The solid histogram shows the SIMC simulation using Eq. 3 and the spectral function of Ref. [39]. The bin widths are the same for the histogram and the data.

We corrected the measured ratio of the normalized yields, $Y_{^3\mathrm{He}}/Y_{^3\mathrm{H}}$, for the radioactive decay of 2.78±0.18% of the target ^{3}H nuclei to ^{3}He in the six months since the target was filled, and denote the corrected yield ratio by $R^{corr.yield}_{^3\mathrm{He}/^3\mathrm{H}}$.

The point-to-point systematical uncertainties on this ratio due to the event selection criteria (momentum and angular acceptances, and θ_{rq} and x_B limits) were extracted by repeating the analysis 5000 times, selecting each criterion randomly within reasonable limits for each iteration. The systematic uncertainty was taken to be the standard deviation of the resulting distribution of ratios. They range from 1% to 8% and are typically much smaller than the statistical uncertainties. See online supplementary materials for details.

Figure 2 shows the missing momentum dependence of the corrected event yield ratio $R^{corr.yield}_{^3\mathrm{He}/^3\mathrm{H}}$ for each kinematical setting. The point-to-point systematic uncertainties are much smaller than the statistical ones. There is an overall normalization uncertainty of 1.8% predominantly due to the target density uncertainty. Other normalization uncertainties due to beam-charge measurement and run-by-run stability are at the 1% level or lower, see Table I.

The data are compared to the PWIA spectral-function based SIMC calculation. The calculation agrees with the measured ratio up to 250 MeV/c, and underpredicts it by $20-50\%$ at higher momenta.

To extract the experimental cross-section ratio, $\sigma_{^3\text{He}(e,e'p)}/\sigma_{^3\text{H}(e,e'p)}(p_{miss})$, we corrected the measured yield ratio $R^{corr.yield}_{^3\text{He}/^3\text{H}}$ for radiative and bin-migration effects as well as for the finite missing-energy acceptance of the spectrometers. The latter equals the calculated momentum distribution ratio divided by the calculated ratio of spectral functions integrated over the missing energy acceptance. The correction factors were calculated using SIMC and found to be smaller than 10% for all p_{miss} values in either kinematics (both the individual corrections and the total correction). We apply a point-to-point systematic uncertainty of 20% of the resulting correction factors. See Table I and online supplementary material for details.

We also calculated the effects of final state interactions using a computer code developed by M. Sargsian [44]. It includes single rescattering of the knocked-out proton with either of the two other nucleons in the three-body-breakup reaction using the generalized Eikonal approximation [45, 46]. For each bin we calculated both the PWIA and FSI cross section, integrated over the experimental acceptance and formed the double ratio

$$R^{FSI} = \frac{\sigma_{FSI}/\sigma_{PWIA}|_{^3\text{He}}}{\sigma_{FSI}/\sigma_{PWIA}|_{^3\text{H}}}.$$

We found that the FSI effects on the individual ^{3}He and $^3\text{H}(e,e'p)$ cross-sections varied between 10% and 30% relative to PWIA, and largely cancel in the ratio, producing at most a 5% effect at the highest p_{miss} kinematics. This reinforces the claim that FSI effects are very small in the cross-section ratio. We did not correct the data for FSI. See online supplementary materials for more information.

Furthermore, we tested the cross section factorization approximation by comparing the factorized spectral function approach used in SIMC with a non-factorized calculation by J. Golak [47–49]. The difference between the factorized and non-factorized calculations was about 5%, which is not enough to explain the data-calculation discrepancy at high p_{miss}.

Figure 3 shows the p_{miss} dependence of the extracted ^{3}He / ^{3}H $(e,e'p)$ cross-section ratio. In the simplest model, this ratio should equal two, the relative number of protons in ^{3}He and ^{3}H. However, we expect that at large p_{miss} the ratio will equal one, the relative number of np SRC pairs in ^{3}He and ^{3}H [50–58]. These SRC pairs will shift equal amounts of cross-section strength from low p_{miss} to high p_{miss} in both nuclei, increasing the ^{3}He to ^{3}H ratio at low p_{miss} to more than two. The measured ratio follows this simple np-SRC expectation,

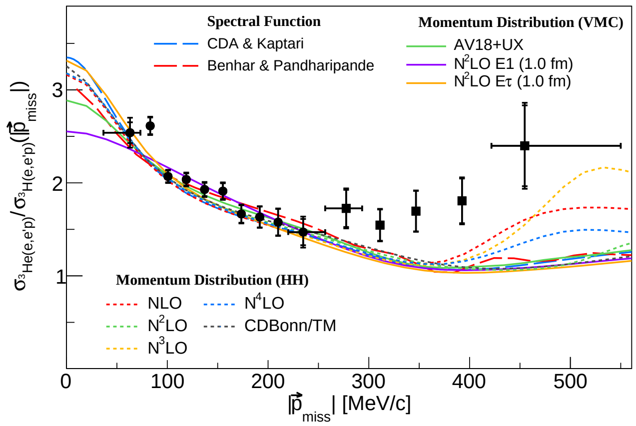

FIG. 3. (color online) Extracted ^{3}He to ^{3}H $(e,e'p)$ cross-section ratio plotted vs. p_{miss} compared with different models of the corresponding momentum distribution ratio. The filled circle and square markers correspond to the low and high p_{miss} settings respectively. Uncertainties shown include both statistics and point-to-point systematics. Common normalization unceraitnty of about 1.8% are not shown (see table I). Horizontal bars indicate the bin sizes and are shown for only the first and last points in each kinematical setting as all other points are equally spaced. The theoretical calculations are done using different local and non-local interactions, as well as different techniques for solving the three-body problem. See text for details.

decreasing from almost three at low p_{miss} towards about 1.5 at $p_{miss} = 250$ MeV/c. At larger p_{miss} the measured ratio is approximately flat, however there is a 20 - 50% difference between the data and the PWIA expectation. This is much larger than the calculated $\leq 5\%$ effects of FSI described above.

With the missing-energy acceptance correction and the small FSI effects, the resulting cross-section ratio should be sensitive to the ratio of momentum distributions. We therefore compare in Fig. 3 the measured ^{3}He/^{3}H $(e,e'p)$ cross-section ratio directly with the ratio of various ^{3}He/^{3}H single-nucleon momentum distributions. The ^{3}H and ^{3}He momentum distribution calculations shown in Fig. 3 are obtained using either the variational Monte Carlo (VMC) technique with local interactions [43, 59] or the Hyperspherical Harmonics (HH) method [60, 61] with non-local interaction.

Local interactions used include the phenomenological AV18 [2] two-nucleon potential augmented by the Urbana X (UX) [62] three-nucleon force and the chiral effective field theory potentials at N^{2}LO (including two- and three-body contributions) Refs. [63–67], using a coordinate-space cutoff of 1 fm and different parametrizations of the three-body contact term $E\tau$ and $E1$. Non-local interactions include the meson-theoretic CD-Bonn [68] two-nucleon potential, together with the Tucson-Melbourne [69] (TM) three-nucleon potential, or the latest chiral two-body potentials from NLO to N^{4}LO

TABLE I. Systematic uncertainties in the extraction of the ^{3}He / ^{3}H $(e,e'p)$ normalized event-yield, $R^{corr.yield}_{^3\mathrm{He}/^3\mathrm{H}}$, (Fig. 2) and cross-section, $\sigma_{^3\mathrm{He}(e,e'p)}/\sigma_{^3\mathrm{H}(e,e'p)}$, (Fig. 3) ratios. Uncertainties marked by '*' contribute only to the cross-section ratio. All uncertainties are summed in quadrature. See text for details.

	Overall	Point-to-point
Target Walls	$\ll 1\%$	
Target Density	1.5%	
Beam-Charge and Stability	1%	
Tritium Decay	0.18%	
Cut sensitivity		1% - 8%
Simulation Corrections* (bin-migration, radiation, E_m acceptance)		1% - 2%

[70], including three-nucleon interactions. The main contribution to the latter, namely the one arising from two-pion exchange, is effectively included at the same chiral order as the two-nucleon interaction Refs. [61, 70]. In these calculation the momentum-space cutoff Λ is kept fixed at 500 MeV. The VMC calculations using the AV18 and UX interactions produce equivalent results as the HH calculations using the AV18 plus Urbana IX [71] interactions.

For completeness Fig. 3 also shows the momentum-distribution ratio calculated by integrating over the missing energy in the spectral functions of Ref. [39] and Ref. [72], obtained using the AV18 two-nucleon only and the AV14 [73] two- and the Urbana VIII [74] (UVIII) three-nucleon interactions, respectively.

All calculated momentum-distribution ratios shown agree with the data up to $p_{miss} \approx 250$ MeV/c. At larger p_{miss}, the theoretical predictions obtained by integrating the spectral functions or by calculating the momentum distribution ratio with local potentials or with the CD-Bonn/TM model disagree with the data by 20–50%. In the case of the non-local chiral potential models, the calculations show significant order dependence.

While momentum distributions calculated with local chiral-interactions depend strongly on the cutoff parameter, these effects appear to mostly cancel in the ratio of the momentum distributions [75].

While FSI calculated in the generalized Eikonal approximation are small, more complete calculations are needed, including two- and three-body interaction operators [76], to determine if the discrepancy between data and calculation is due to the reaction mechanism or to the validity of the underlying NN potentials at short-distances.

To summarize, we presented the first measurement of the ^{3}He$(e,e'p)$ and ^{3}H$(e,e'p)$ reactions in kinematics where the cross-sections are expected to be sensitive to the proton momentum distribution, i.e., at large Q^2, $x_B > 1$, and $\theta_{rq} < 40°$ that minimize two-body currents and the effects of FSI. We further enhanced the sensitivity to the momentum distribution by extracting the ratio of the cross-sections, so that most of the remaining FSI effects cancel, as confirmed by a generalized Eikonal approximation calculation of leading proton rescattering.

While the measured corrected cross-section ratio $\sigma_{^3\mathrm{He}(e,e'p)}/\sigma_{^3\mathrm{H}(e,e'p)}$ is well described by PWIA calculations up to $p_{miss} \approx 250$ MeV/c, they disagree by only 20 - 50% at high p_{miss}, despite a four order of magnitude decrease of the momentum distribution in this range. This is a vast improvement over previous $\sigma_{^3\mathrm{He}(e,e'p)}$ measurements at lower Q^2 and $x_B = 1$, which disagreed with PWIA calculations by factors of several at large p_{miss} [21, 22]. This, together with FSI calculations, strongly supports the reduced contribution of non-QE reaction mechanisms in our kinematics.

The data overall supports the transition from single-nucleon dominance at low p_{miss}, towards an np-SRC pair dominant region at high p_{miss} [50–58]. However, more complete calculations are needed to assess the implications of the observed 20–50% deviation of the data from the PWIA calculation in the expected np-SRC pair dominance region. If the observed difference between the ^{3}He/^{3}H experimental ratio and momentum distribution ratios at large missing momenta is due to the underlying NN interaction, then it can provide significant new constraints on the previously loosely-constrained short-distance parts of the NN interaction.

We acknowledge the contribution of the Jefferson-Lab target group and technical staff for design and construction of the Tritium target and their support running this experiment. We thank C. Degli-Atti and L. Kaptari for the ^{3}He spectral function calculations and M. Sargsian, M. Strikman, J. Carlson, S. Gandolfi, R. B. Wiringa, for many valuable discussions. This work was supported by the U.S. Department of Energy (DOE) grant DE-AC05-06OR23177 under which Jefferson Science Associates, LLC, operates the Thomas Jefferson National Accelerator Facility, the U.S. National Science Foundation, the Pazi foundation, the Israel Science Foundation, and the NUCLEI SciDAC program. Computational resources for the calculation of the N^{2}LO momentum distributions have been provided by Los Alamos Open Supercomputing via the Institutional Computing (IC) program and by the National Energy Research Scientific Computing Center (NERSC), which is supported by the U.S. Department of Energy, Office of Science, under Contract No. DE-AC02-05CH11231. The Kent State University contribution is supported under the PHY-1714809 grant from the U.S. National Science Foundation. The work of ANL group members is supported by DOE grant DE-AC02-06CH11357.

[1] R. Machleidt, K. Holinde, and C. Elster, Phys. Rept. **149**, 1 (1987).
[2] R. B. Wiringa, V. G. J. Stoks, and R. Schiavilla, Phys. Rev. C **51**, 38 (1995), arXiv:nucl-th/9408016 [nucl-th].
[3] E. Epelbaum, H.-W. Hammer, and U.-G. Meißner, Rev. Mod. Phys. **81**, 1773 (2009).
[4] R. Machleidt and D. R. Entem, Phys. Rep. **503**, 1 (2011).
[5] E. Epelbaum, H.-W. Hammer, and U.-G. Meissner, Rev. Mod. Phys. **81**, 1773 (2009), arXiv:0811.1338 [nucl-th].
[6] J. Carlson and R. Schiavilla, Rev. Mod. Phys. **70**, 743 (1998).
[7] J. Carlson, S. Gandolfi, F. Pederiva, S. C. Pieper, R. Schiavilla, K. E. Schmidt, and R. B. Wiringa, Rev. Mod. Phys. **87**, 1067 (2015), arXiv:1412.3081 [nucl-th].
[8] M. Piarulli, L. Girlanda, R. Schiavilla, A. Kievsky, A. Lovato, L. E. Marcucci, S. C. Pieper, M. Viviani, and R. B. Wiringa, Phys. Rev. C **94**, 054007 (2016).
[9] G. Hagen, T. Papenbrock, M. Hjorth-Jensen, and D. J. Dean, Reports on Progress in Physics **77**, 096302 (2014).
[10] B. R. Barrett, P. Navrátil, and J. P. Vary, Progr. Part. Nucl. Phys. **69**, 131 (2013).
[11] O. Hen, G. A. Miller, E. Piasetzky, and L. B. Weinstein, Rev. Mod. Phys. **89**, 045002 (2017), arXiv:1611.09748 [nucl-ex].
[12] C. Ciofi degli Atti, Phys. Rept. **590**, 1 (2015).
[13] B. Schmookler, M. Duer, A. Schmidt, *et al.* (CLAS), Nature **In Print** (2019).
[14] J.-W. Chen, W. Detmold, J. E. Lynn, and A. Schwenk, Phys. Rev. Lett. **119**, 262502 (2017), arXiv:1607.03065 [hep-ph].
[15] L. B. Weinstein, E. Piasetzky, D. W. Higinbotham, J. Gomez, O. Hen, and R. Shneor, Phys. Rev. Lett. **106**, 052301 (2011), arXiv:1009.5666 [hep-ph].
[16] O. Hen, E. Piasetzky, and L. B. Weinstein, Phys. Rev. **C85**, 047301 (2012), arXiv:1202.3452 [nucl-ex].
[17] O. Hen, D. W. Higinbotham, G. A. Miller, E. Piasetzky, and L. B. Weinstein, Int. J. Mod. Phys. **E22**, 1330017 (2013), arXiv:1304.2813 [nucl-th].
[18] L. Frankfurt, M. Sargsian, and M. Strikman, Int. J. Mod. Phys. A **23**, 2991 (2008), arXiv:0806.4412 [nucl-th].
[19] B.-A. Li, B.-J. Cai, L.-W. Chen, and J. Xu, Prog. Part. Nucl. Phys. **99**, 29 (2018), arXiv:1801.01213 [nucl-th].
[20] A. Bussiere, J. Mougey, D. Royer, D. Tarnowski, S. Turck-Chieze, M. Bernheim, S. Frullani, G. P. Capitani, E. De Sanctis, and E. Jans, Nucl. Phys. **A365**, 349 (1981).
[21] F. Benmokhtar *et al.* (Jefferson Lab Hall A), Phys. Rev. Lett. **94**, 082305 (2005), arXiv:nucl-ex/0408015 [nucl-ex].
[22] M. M. Rvachev *et al.* (Jefferson Lab Hall A), Phys. Rev. Lett. **94**, 192302 (2005), arXiv:nucl-ex/0409005 [nucl-ex].
[23] K. S. Egiyan *et al.* (CLAS), Phys. Rev. Lett. **98**, 262502 (2007), arXiv:nucl-ex/0701013 [nucl-ex].
[24] C. Ciofi degli Atti and L. P. Kaptari, Phys. Rev. Lett. **95**, 052502 (2005), arXiv:nucl-th/0502045 [nucl-th].
[25] J. M. Laget, Phys. Lett. **B609**, 49 (2005), arXiv:nucl-th/0407072 [nucl-th].
[26] M. Alvioli, C. Ciofi degli Atti, and L. P. Kaptari, Phys. Rev. **C81**, 021001 (2010), arXiv:0904.4045 [nucl-th].
[27] W. U. Boeglin *et al.* (Hall A), Phys. Rev. Lett. **107**, 262501 (2011), arXiv:1106.0275 [nucl-ex].
[28] J. J. Kelly, Adv. Nucl. Phys. **23**, 75 (1996), [,75(1996)].
[29] T. De Forest, Nucl. Phys. A **392**, 232 (1983).
[30] M. M. Sargsian, Int. J. Mod. Phys. **E10**, 405 (2001), arXiv:nucl-th/0110053 [nucl-th].
[31] L. L. Frankfurt, M. M. Sargsian, and M. I. Strikman, Phys. Rev. C **56**, 1124 (1997), arXiv:nucl-th/9603018 [nucl-th].
[32] S. Jeschonnek and J. W. Van Orden, Phys. Rev. C **78**, 014007 (2008), arXiv:0805.3115 [nucl-th].
[33] M. M. Sargsian, Phys. Rev. **C82**, 014612 (2010), arXiv:0910.2016 [nucl-th].
[34] O. Hen, L. B. Weinstein, S. Gilad, and W. Boeglin, "Proton and Neutron Momentum Distributions in A = 3 Asymmetric Nuclei," (2014), arXiv:1410.4451 [nucl-ex].
[35] M. M. Sargsian *et al.*, J. Phys. **G29**, R1 (2003), arXiv:nucl-th/0210025 [nucl-th].
[36] D. Meekins, Jefferson Lab Engineering Report (2017).
[37] S. N. Santiesteban *et al.*, (2018), arXiv:1811.12167 [physics.ins-det].
[38] "SIMC," `https://hallcweb.jlab.org/wiki/index.php/SIMC_Monte_Carlo`, Accessed: 2018-10-11.
[39] C. Ciofi degli Atti and L. P. Kaptari, Phys. Rev. C **71**, 024005 (2005), arXiv:nucl-th/0407024 [nucl-th].
[40] J. Alcorn *et al.*, Nucl. Instrum. Meth. **A522**, 294 (2004).
[41] "In 2016, the Quadrupole magnet closest to the target (Q1) was replaced with a normal conducting quad, with similar magnetic properties.".
[42] E. L. Lomon, (2006), arXiv:nucl-th/0609020 [nucl-th].
[43] R. B. Wiringa, R. Schiavilla, S. C. Pieper, and J. Carlson, Phys. Rev. C **89**, 024305 (2014).
[44] "M. Sargsian, Private communication,".
[45] M. M. Sargsian, T. V. Abrahamyan, M. I. Strikman, and L. L. Frankfurt, Phys. Rev. C **71**, 044614 (2005).
[46] M. M. Sargsian, T. V. Abrahamyan, M. I. Strikman, and L. L. Frankfurt, Phys. Rev. C **71**, 044615 (2005).
[47] C. Carasco *et al.*, Physics Letters B **559**, 41 (2003).
[48] J. Bermuth *et al.*, Physics Letters B **564**, 199 (2003).
[49] J. Golak, R. Skibinski, H. Witala, W. Glockle, A. Nogga, and H. Kamada, Phys. Rept. **415**, 89 (2005), arXiv:nucl-th/0505072 [nucl-th].
[50] R. Weiss, R. Cruz-Torres, N. Barnea, E. Piasetzky, and O. Hen, Phys. Lett. **B780**, 211 (2018), arXiv:1612.00923 [nucl-th].
[51] E. Piasetzky, M. Sargsian, L. Frankfurt, M. Strikman, and J. W. Watson, Phys. Rev. Lett. **97**, 162504 (2006).
[52] A. Tang *et al.*, Phys. Rev. Lett. **90**, 042301 (2003).
[53] R. Shneor *et al.*, Phys. Rev. Lett. **99**, 072501 (2007).
[54] R. Subedi *et al.*, Science **320**, 1476 (2008).
[55] I. Korover, N. Muangma, O. Hen, *et al.*, Phys. Rev. Lett. **113**, 022501 (2014).
[56] O. Hen *et al.*, Science **346**, 614 (2014), arXiv:1412.0138 [nucl-ex].
[57] M. Duer *et al.* (CLAS), Nature **560**, 617 (2018).
[58] M. Duer, O. Hen, E. Piasetzky, L. B. Weinstein, A. Schmidt, I. Korover, E. O. Cohen, and H. Hakobyan (CLAS), (2018), arXiv:1810.05343 [nucl-ex].
[59] D. Lonardoni, S. Gandolfi, X. B. Wang, and J. Carlson, Phys. Rev. C **98**, 014322 (2018).
[60] A. Kievsky, S. Rosati, M. Viviani, L. E. Marcucci, and L. Girlanda, J. Phys. **G35**, 063101 (2008), arXiv:0805.4688 [nucl-th].
[61] L. E. Marcucci, F. Sammarruca, M. Viviani, and R. Machleidt, (2018), arXiv:1809.01849 [nucl-th].
[62] R. B. Wiringa, *Single-Nucleon Momentum Distributions*, `http://www.phy.anl.gov/theory/research/momenta`

(2018), last update: August 6, 2018.
[63] A. Gezerlis, I. Tews, E. Epelbaum, M. Freunek, S. Gandolfi, K. Hebeler, A. Nogga, and A. Schwenk, Phys. Rev. C **90**, 054323 (2014).
[64] J. E. Lynn, I. Tews, J. Carlson, S. Gandolfi, A. Gezerlis, K. E. Schmidt, and A. Schwenk, Phys. Rev. Lett. **116**, 062501 (2016).
[65] J. E. Lynn, I. Tews, J. Carlson, S. Gandolfi, A. Gezerlis, K. E. Schmidt, and A. Schwenk, Phys. Rev. C **96**, 054007 (2017).
[66] D. Lonardoni, J. Carlson, S. Gandolfi, J. E. Lynn, K. E. Schmidt, A. Schwenk, and X. B. Wang, Phys. Rev. Lett. **120**, 122502 (2018).
[67] D. Lonardoni, S. Gandolfi, J. E. Lynn, C. Petrie, J. Carlson, K. E. Schmidt, and A. Schwenk, Phys. Rev. C **97**, 044318 (2018).
[68] R. Machleidt, Phys. Rev. **C63**, 024001 (2001), arXiv:nucl-th/0006014 [nucl-th].
[69] S. A. Coon and H. K. Han, Few Body Syst. **30**, 131 (2001), arXiv:nucl-th/0101003 [nucl-th].
[70] D. R. Entem, R. Machleidt, and Y. Nosyk, Phys. Rev. **C96**, 024004 (2017), arXiv:1703.05454 [nucl-th].
[71] B. S. Pudliner, V. R. Pandharipande, J. Carlson, and R. B. Wiringa, Phys. Rev. Lett. **74**, 4396 (1995), arXiv:nucl-th/9502031 [nucl-th].
[72] O. Benhar and V. R. Pandharipande, Phys. Rev. **C47**, 2218 (1993).
[73] R. B. Wiringa, R. A. Smith, and T. L. Ainsworth, Phys. Rev. **C29**, 1207 (1984).
[74] J. Carlson, V. R. Pandharipande, and R. B. Wiringa, Nucl. Phys. **A401**, 59 (1983).
[75] D. Lonardoni, S. Gandolfi, X. B. Wang, and J. Carlson, Phys. Rev. C **98**, 014322 (2018), arXiv:1804.08027 [nucl-th].
[76] S. N. More, S. K. Bogner, and R. J. Furnstahl, Phys. Rev. C **96**, 054004 (2017).